Meso-scale modeling of concrete: a morphological description based on excursion sets of Random Fields.

Emmanuel Roubin[a,*], Jean-Baptiste Colliat[b], Nathan Benkemoun[c]

[a] *International Center for Numerical Methods in Engineering (CIMNE)*
Campus Nord UPC, Edifici C-1, c/ Jordi Girona 1-3, 08034 Barcelona, SPAIN.
[b] *Laboratoire de Mécanique de Lille,*
Université Sciences et Technologies Lille 1, CNRS, Ecole Centrale de Lille, Arts et Métiers ParisTech
Boulevard Paul Langevin, Cité Scientifique, 59655 Villeneuve d'Ascq Cedex, FRANCE
[c] *Université Nantes Angers Le Mans (L'UNAM), GeM,*
Research Institute of Civil Engineering and Mechanics, CNRS UMR 6183, Nantes University, IUT Saint-Nazaire
58 rue Michel Ange, 44600 Saint-Nazaire, FRANCE

Abstract

In view of the significant impact of thin scale heterogeneities in regards with the macroscopic response of concrete (and generally speaking of heterogeneous materials), a particular effort is dedicated to morphological representation and modeling. The development of a model based on spatially correlated random functions (Random Fields) is proposed in this article. It is shown how the stationary ergodic property coupled with the spatial structure of correlated Random Fields can efficiently address the problematic when submitted to a threshold process. Recent mathematical results Adler (2008) give accurate ways to analytically control the resulting morphology, both geometrically and topologically speaking. The generalized aspect of this framework has to be seen here as the ability of the model to represent different kind of morphologies such as matrix/inclusion, opened or closed porosity. With such features, heterogeneous material can be represented at different scales. By expanding a rather abstract formula given by Adler (2008), the authors aim at spreading this point of view with a "ready for use" framework. Furthermore, by addressing common issues such as, reaching high volume fraction with disconnected topologies and representing grain size distributions, solutions to adapt it to cementitious materials are given.

Keywords: Cementitious material, morphological modeling, correlated Random Fields, excursion sets.

1. Introduction

One of the fundamental task of materials science is to – quantitatively – relate fine scale information (*e.g.* microstructure morphology) to macroscopic properties. To this aim

*Corresponding author.
Email address: eroubin@cimne.upc.edu (Emmanuel Roubin)

a huge effort has been paid during the last decade to set up numerical simulations that are able to take into account for this fine scale information (Zhu et al. (2008); Wriggers and Moftah (2006); Garboczi and Bentz (1998); Zubelewicz et al. (2014)). Of course this effort is concomitant with the spread of three-dimensional and non-destructive experiments such as X-ray microtomography, which provides some of the morphological data that the numerical simulations require (Rougelot et al. (2010)).

Cement-based materials, whether cement paste, mortar, concrete or high performance concrete is considered, are heterogeneous materials that exhibit complex and random morphologies over a wide range of length scales. Therefore it is a large and difficult task to try to link microstructure at a certain scale to properties at the upper one.

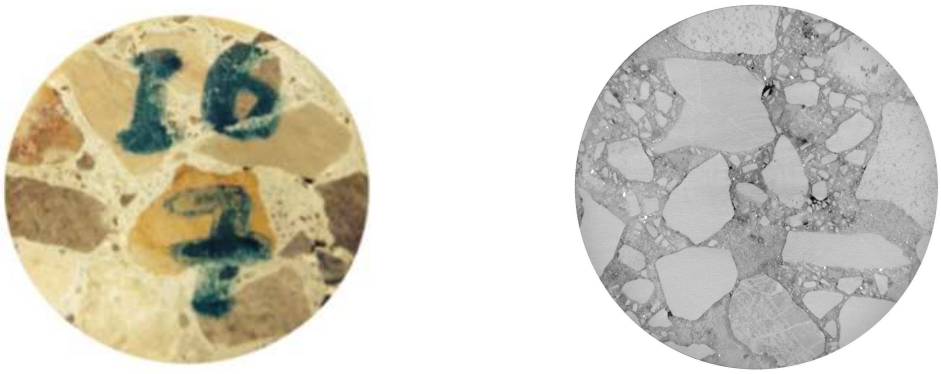

(a) Optical photography. (b) X-ray tomography.

Figure 1: Meso-scale point of view for concrete: slices of diameter $8\,mm$ from Qier (2014)

Here focus is made on the so-called meso-scale (Fig. (1)) that, basically, is the scale for which heterogeneities larger than one millimeter can be seen. At such scale concrete can be seen as aggregates and large sand particles melt into a mortar matrix (cement paste and sand particles). Indeed, explicitly take into account for these heterogeneities within numerical simulations offer a wide range of new possibilities such as (i) the introduction of some specific (*e.g.* non-linear) behavior for the interfaces, (ii) the computation of some structural effect due to the gathering of several components with different mechanical (not only elastic) properties. Recently, it has been shown (Roubin et al. (2015)) that these new abilities may lead to the emergence, at the macro-scale, of some non-linear mechanical behavior (*e.g.* failure in uniaxial or triaxial compression) that were not introduced among the set of fine scale mechanisms. Indeed the quality of the morphological representation is the cornerstone of this methodology and our main motivation here is to focus on a very general and simple way to model concrete at meso-scale.

This "generalized" morphological model relies on the excursion set theory of correlated Random Fields. Here, the term "generalized" has to be thought as the ability of the model to represent, with the same theoretical basis, several kinds of morphologies (*e.g.* matrix/inclusion, porous media, *etc*) that may turn out to be a handy tool when cementitious materials are considered for different observation scales. Compared to hard spheres packing's

(Bezrukov et al. (2002)), it will be shown that the excursion sets lead to some straightforward numerical implementations and very low data storage. This point is a major advantage when dealing with fine — more than one million nodes — grids.

Basically an excursion set is the thresholding process of a random function defined over a finite space M. For example, if $g(\boldsymbol{x}) : M \subset \mathbb{R}^3 \to \mathbb{R}$ is a realization of a random function (see FIG. (2(a)), then for a given threshold (hereafter called threshold) κ, the excursion set $E_s \subset \mathbb{R}^3$ (see FIG. (2(b))) can be defined by the part of M where g is greater than κ,

$$E_s = \{\boldsymbol{x} \in M \mid g(\boldsymbol{x}) > \kappa\}\,.$$

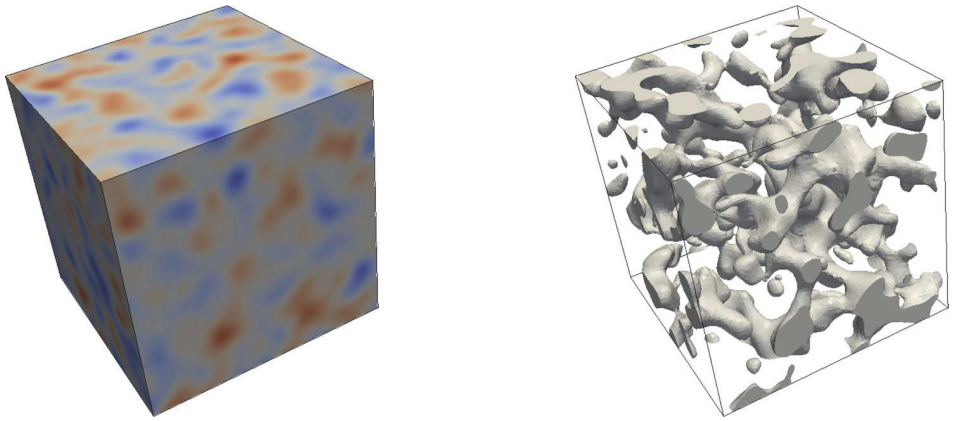

(a) $g(\boldsymbol{x})$ — Realization of a correlated Random Field (Gaussian).

(b) E_s — Resulting excursion set for a given threshold (larger than zero).

Figure 2: Illustration of the excursion set principle.

As shown in FIG. (2), excursion sets can have very different aspects depending on the chosen threshold and the random function characteristics. Henceforth, it seems relevant to use them in the context of correlated Random Fields since their intrinsic spatial structure — through covariance functions — leads to complex shapes and flexible structures that can be statistically controlled both geometrically and topologically speaking. Indeed, as mentioned in Serra (1982) and Roberts and Garboczi (1999) for cementitious materials, the strength of this theory relies in its control of morphologies through global descriptors (volume, surface, number and size of connected components). Indeed, these quantities are Random Variables. Here, the morphological model is based on a formula from Adler (2008) that provides the expectations of these variables, granting a powerful predictive aspect to the model.

Basically this paper attempts to present in detail this theory along with its adaptation to cementitious materials. For that matter, the first section covers both theoretical and numerical basis of the excursion sets theory. Then, mathematical tools to characterize morphologies along with the main results of Adler (2008) are presented. Based on recommendations made in the latter publication, an helpful extension of the basic result is proposed through a rather general formula. In the last section, applications related to cementitious materials observed at the meso-scale are proposed. The main one consists in using the model through union

of excursion sets in order to represent size distributed aggregates that are included within a coarse mortar matrix. For that matter, the problematic of reaching high fraction volumes with disconnected topology is addressed in detail along with the use of the excursion set theory applied to χ^2 distribution.

2. Excursion set as a tool for morphological modeling

The use of correlated Random Fields (hereafter RF) brings a major improvement to morphological modeling. Indeed, in addition to the usual characteristics of Random Variables such as mean or variance, the *correlated* aspect gives a spatial structure to the fields which can be defined by covariance functions[1]. It is through this statistical control that excursion sets of certain correlated RFs have interesting properties, such as predictable geometrical and topological characteristics.

This section first defines the mathematical framework of excursion sets and its scope, then addresses some remarks regarding covariance functions and finally gives details on the measures characterizing these excursions.

2.1. General principle of excursion sets

An excursion set is defined as the resulting subset of a thresholding operation of a correlated RF. Basically, this operation transforms a continuous field (RF) to a binary one (excursion), creating randomly shaped morphologies. If $g : M \subset \mathbb{R}^N \to \mathbb{R}$ is a RF defined over parameter space M (bounded region of $\mathbb{R}^N$), a subset of its co-domain $H_s \subset \mathbb{R}$ can be defined in order to set the thresholding rules. Herein, excursion sets, noted E_s, are defined as the set of points where the RF value is in H_s, hereafter called *hitting set*. Thus yielding to:

$$E_s \triangleq \{\boldsymbol{x} \in M \mid g(\boldsymbol{x}) \in H_s\}. \tag{1}$$

The hitting set will often be taken as the open set $H_s = [\kappa, \infty)$, κ working as a threshold. Each point where the RF value is above κ defines the excursion. Thus Eq. (1) can simply be written:

$$E_s(\kappa) \triangleq \{\boldsymbol{x} \in M \mid g(\boldsymbol{x}) \geq \kappa\}. \tag{2}$$

This principle is depicted in Fig. (3) in the one-dimensional case and examples of three-dimensional excursions are given in Fig. (4) for two different thresholds. In the presented study, the RF is defined over a three-dimensional space ($M \subset \mathbb{R}^3$), creating three-dimensional excursion sets. The two excursions of Fig. (4) are made from the same realization of a RF with two different thresholds. Threshold value has clearly an important impact on the resulting morphology. For low values of κ, a major part of the field still hits H_s, leading to high volume fraction excursion set mainly made of cavities and handles. This sponge-like topology (Fig. (4(a))) can be a suitable representation of porous media. By comparison, high values of κ lead to meatball-like topology (Fig. (4(b))) where

[1]For readers not familiar with correlated RFs, it is recommended to read the walk-through details given in Roubin (2013) or any other book on the topic like Rasmussen and Williams (2006).

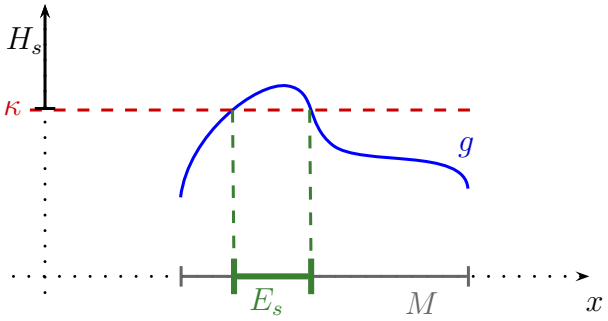

Figure 3: Excursion set of correlated RF in one-dimension.

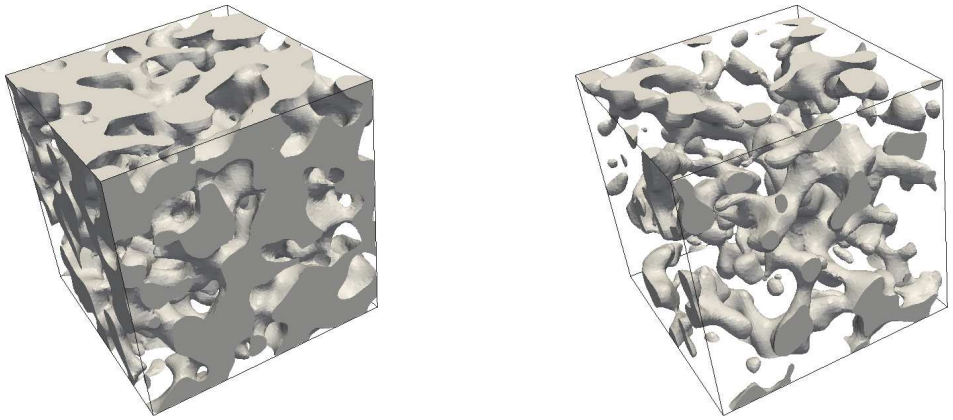

(a) Porous media (low threshold). (b) Matrix/inclusion media (large threshold).

Figure 4: Two excursion sets of the same realization with different thresholds.

just several connected components remain. These excursions, despite their very low volume fraction, could represent disconnected media such as aggregates within a matrix. This last point raises a main issue of excursion set modeling. In this paper, solutions are proposed in order to yield morphologies with high volume fraction morphologies and still disconnected topologies.

As the threshold value has an impact on the kind of morphology obtained, both probability distribution of the RF and its covariance function have a major influence as well. Among them, the correlation length l_c, fixing the length-scale of the excursion set, has a key role. But before giving details on this latter property, attention is first driven to the scope of this framework.

2.2. Scope of the theoretical framework

Although throughout this paper, application is mainly be driven with Gaussian and χ^2 distributions and Gaussian covariance functions, it is important to remind that this theory holds for much more general cases.

First, in regards with the *distribution*, the whole set of Gaussian related RF can be used.

If g_r is such field, it is defined by:

$$g_r : \Omega \times \mathbb{R}^N \xrightarrow{\boldsymbol{g}} \mathbb{R}^k \xrightarrow{S} \mathbb{R}, \tag{3}$$

where $\boldsymbol{g} = \{g_i\}, i = [1..k]$ is a vector valued Gaussian RF (*i.e.* all g_i are independent). For example, with $S(\boldsymbol{g}) = \|\boldsymbol{g}\|_2$, χ^2_k distribution can be used or with $k = 1$ and $S(g) = \exp(g)$, log-normal ones. This generalization can be understood, as in Adler (2008), by the following decomposition showing that the probability of g_r to hit H_s falls down to the probability of $\boldsymbol{g}$ to hit $S^{-1}(H_s)$:

$$P\left\{g_r \in H_s\right\} = P\left\{S(\boldsymbol{g}) \in H_s\right\} = P\left\{\boldsymbol{g} \in S^{-1}(H_s)\right\}. \tag{4}$$

Then, in regards with the *spatial structure*, the only requirement is to use mean-square differentiable RFs. More details are given in Adler (1981); Rasmussen and Williams (2006) on this property linked with the covariance function. It is worth noting that finding the proper RF in order to yield the desired excursion require a *functional* analysis and not just a parameter optimization.

For the sake of clarity, it is the authors choice to omit this extended scope. Interested readers are invited to read Roubin (2013).

2.3. The role of the covariance function

Several properties of the covariance function are worth noticing, the most common being the correlation length (noted l_c). As depicted in Fig. (5), it is a direct way of controlling the so called spatial structure. It can be seen that it sets a scale factor between the field structure (distance between local extrema) and the domain size.

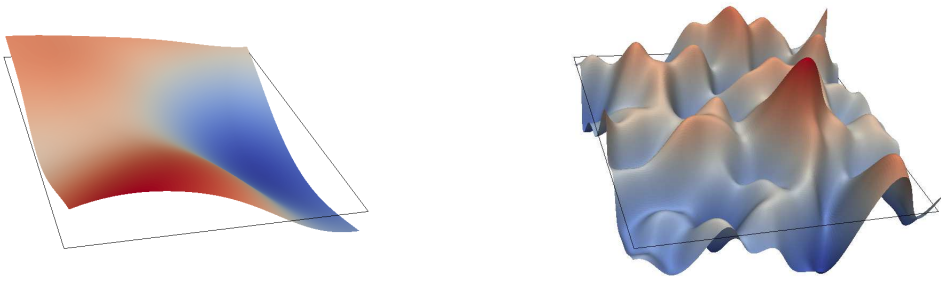

(a) Large l_c (equal to the domain size). (b) Small l_c (one-tenth of the domain size).

Figure 5: Impact of the correlation length l_c on two realizations of Gaussian RFs with Gaussian covariance functions.

Intimately linked with the present framework, another way of understanding the role of the correlation length is through the number of up-crossings $\mathcal{N}$ of a threshold κ. For a

one-dimensional RF, the expected number of up-crossings $\mathbb{E}\{\mathcal{N}(\kappa)\}$ of the threshold κ can be determined for a stationary zero mean correlated Gaussian RFs yielded over a segment of size a. Actually its value only depends on the underlying spectral moments λ_0 and λ_2 (see Adler et al. (2010)). For a Gaussian covariance function of variance σ^2, $\lambda_0 = \sigma^2$ and $\lambda_2 = 2\sigma^2/l_c^2$ and the expected value of the number of up-crossings is computed:

$$\mathbb{E}\{\mathcal{N}(\kappa)\} = \frac{a}{2\pi}\sqrt{\frac{\lambda_2}{\lambda_0}}\exp\left(-\frac{\kappa^2}{2\lambda_0}\right) = \frac{a}{\sqrt{2}\pi l_c}\exp\left(-\frac{\kappa^2}{2\sigma^2}\right). \tag{5}$$

Illustrating the length-scale role of l_c, it can be seen that it decreases hyperbolically as the correlation length increases. In addition to its depicting nature, Eq. (5) is actually a fundamental base of the excursion set theory presented below. It is worth noting that, with it, the full knowledge of the covariance function is not necessary to predict characteristics such as the number of up-crossings of thresholds. In fact, it is also the case for other characteristics such as the volume, the surface or the Euler characteristic of complex morphologies in higher space dimensions.

However, it is well admitted in the morphological community that infinitely smooth RFs —such as those defined with Gaussian covariance functions— hardly possess any realistic meaning (Stein (1999)). It is reminded to the reader that the full study can easily be extended to other cases, such as using the Matérn class. This latter class changes the modelling at a smaller scale providing the model with a way to represent the roughness of a surface (Rasmussen and Williams (2006)). Thus, it is omitted for the time being.

Focus is now driven to functionals that measure both geometrical and topological quantities. They provide global descriptors for excursion sets, giving a mathematical basis for the main results presented in this paper.

2.4. Geometrical and topological characterization

As an inner requirement of any morphological model, the *geometrical* and *topological* characterization of the morphology (excursion) have to be considered. It has been proved that in a N-dimensional space, $N + 1$ descriptors are enough to fully describe it (Matheron (1975)). Therefore, in the three-dimensional Euclidean space $\mathbb{R}^3$, an excursion is fully characterized by a set of four descriptors: three geometrical and one topological.

A specification of these descriptors is made here through the *Lipschitz-Killing curvatures* (hereafter LKCs) Federer (1959), noted $\mathscr{L}_j$ for $j = [0..3]$, that can be interpreted as the j^{th} measures of the excursion. These descriptors provide the model with physically relevant and useful control since $\mathscr{L}_3$ stands for the volume, $\mathscr{L}_2$ half the surface area, $\mathscr{L}_1$ a length[2] and $\mathscr{L}_0$ the Euler characteristic (topological descriptor).

Though the latter measure can be defined in many ways, focus is made here on the computation of the Euler characteristic of M as the following alternative sum of number of

[2]twice the caliper diameter

topological features:

$$\mathscr{L}_0(M) = \chi(M) = \#\{\text{connected component}\} - \#\{\text{handles}\} + \#\{\text{holes}\}. \tag{6}$$

From Eq. (6), the direct link between the Euler characteristic and the description of a material morphology can be made since each topological feature corresponds to a type of media. Indeed, connected components stands for *matrix/inclusion* topology, handles for *open porosity* and holes for *closed porosity*, giving a "universal" aspect to this descriptor.

Morphological models at the meso-scale find there applications in disconnected medias and thus, the Euler characteristics becomes a measure of the number of inclusions (aggregates). Although, an additional information on phase percolation is used in order to ensure a topological consistency of the morphology (see section 4 for details).

In order to measure the probability space, another set of functionals referred to as *Minkowski functionals* are now presented.

2.5. Statistical characterization

More popular than LKCs, Minkowski functionals are used in many fields in order to characterize morphologies. Especially in the astrophysics community (see the pioneer work of Mecke et al. (1994) in which *Steiner's formula* is presented with these functionals) leading to huge amount of literature on the topic Mecke and Wagner (1991); Winitzki and Kosowsky (1997); Kerscher et al. (2001). However, in contrast to LKCs, the Minkowski functionals are not intrinsic. Therefore, they depend on the used measure. This can be seen as a foretaste of how calculating geometrical properties of excursion sets is linked to the probability of a Gaussian Random Variable to be in the so-called hitting set. Hence, focus is drawn here to the following measure of a Gaussian distribution:

$$\gamma_k(A) = P\left\{\boldsymbol{X} \in A\right\} = \frac{1}{\sigma^k(2\pi)^{k/2}} \int_A e^{-\|\boldsymbol{x}\|^2/2\sigma^2} d\boldsymbol{x}, \tag{7}$$

where $\boldsymbol{X} = \{X_i \sim \mathscr{N}(0, \sigma^2)\}$ is a standard Gaussian vector and $A \subset \mathbb{R}^k$. Associated to this measure, the functionals are now called *Gaussian Minkowski functionals* (hereafter GMFs). The main results of Taylor (2006) is to yield a Taylor expansion of tube probability[3] content Eq. (8) for small enough ρ. It can be seen as an extension of the Steiner-Weyls formula, in which γ_k represents the volume in the sense of Gaussian measure (Gaussian volume).

Taylor expansion of tube Gaussian volume

$$\gamma_k(\mathcal{K}(A,\rho)) = \sum_{j=0}^{\infty} \frac{\rho^j}{j!} \mathscr{M}_j^{\gamma_k}(A), \tag{8}$$

where $\mathcal{K}(A,\rho) = \{\boldsymbol{x} \in \mathbb{R}^N \mid \min_{\forall \boldsymbol{y} \in A}(\|\boldsymbol{x} - \boldsymbol{y}\|) \leq \rho\}$ is the tube of A of radius ρ.

[3]This results is a major breakthrough in the morpho-mathematical community. Diffusing its spin-offs to the mechanical community is one of the goal of this article.

By taking $\rho = 0$, it can be concluded that the first GMF is the Gaussian volume of A itself, $\mathscr{M}_0^{\gamma_k}(A) = \gamma_k(A)$. Thanks to the uniqueness of Taylor expansion, the other GMFs can be computed by doing a polynomial coefficients identification between Eq. (8) and a classical Taylor expansion for small ρ of $\gamma_k(\mathcal{K}(A, \rho))$ from Eq. (7).

Two classes of functionals that characterize a morphology have been presented. In the one hand, the LKCs are used in order to characterize the excursion set geometrical and topological properties. On the other hand, the GMFs gather the statistical information of the random distribution. Development and analytical definition are given for hitting set $[\kappa, \infty) \subset \mathbb{R}$ for both Gaussian and χ^2_k distribution in Roubin (2013) but are not mandatory for the good understanding of the following. The next section presents the main result of this paper: a formulae that links the excursion set morphological characteristics (LKCs) to statistical information of the correlated RF and the hitting set.

3. Expectation formula

The use of correlated RFs and excursion sets in order to represents the heterogeneous aspect of a media is far from being an original work and has been used since decades. However, the originality of this paper resides in this section where a new result from the mathematical community —way more general than depicted here— enhances these frameworks with an analytical way of *controlling* the expected characteristics (LKCs) of the excursion.

The result presented in this section is of fundamental importance in this paper. It is the basis of the work of Taylor (2001); Taylor and Adler (2003); Taylor (2006). It links the statistical information of the distribution used, the hitting set (via the GMFs) and the spatial structure of the correlated RF (via its covariance function second spectral moment) to the geometrical and topological characteristics of the excursion set (via LKCs). Since excursion sets are the results of a threshold of RFs *realizations*, naturally, the LKCs has to be seen in terms of expected values $\mathbb{E}$ (means). Basically, this section defines the F function of the following equation:

$$\mathbb{E}\{\mathscr{L}_j(E_s)\} = F(H_s, \mathcal{C}, S), \tag{9}$$

in which $\mathscr{L}_j$ is the j^{th} LKC, E_s, the excursion set, H_s, the hitting set, $\mathcal{C}$ the covariance function of the correlated RF (containing information on the distribution and the spatial structure) and S the function defining Gaussian related distributions.

3.1. A first taste of the formula

It has been seen that the GMFs are measures of the probabilistic space. Furthermore, the first functional has been identified as the Gaussian measure itself γ_k. This measure only provides information on the distribution and not on the spatial structure of correlated RFs. Nonetheless, the computation of the expectation of the last LKC of an excursion set (volume) can be done while only knowing this.

If $\boldsymbol{g}$ is a stationary correlated Gaussian RF, at any point $\boldsymbol{x} \in M$, it can be seen as a Random Variable with the same given marginal distribution. Hence, the probability of this

point to be part of the excursion set (*i.e.* that $\boldsymbol{g}(\boldsymbol{x}) \in H_s$) is equal to the Gaussian measure of the hitting set, thus yielding to:

$$\forall \boldsymbol{x} \in M, \quad P\{\boldsymbol{g}(\boldsymbol{x}) \in H_s\} = \gamma_k(H_s) = \mathscr{M}_0^{\gamma_k}(H_s). \tag{10}$$

The first GMF can be seen as a local descriptor of the excursion set volume. Notice that it does not depend on $\boldsymbol{x}$, making it trivial to integrate over M. This property can be used in order to calculate the volume of the corresponding excursion set. Since the marginal distribution is constant over M it can be yielded by simply multiplying the probability of each point to be in H_s by the volume of M; $\mathscr{L}_N(M)$. It leads, for the more general case of Gaussian related RF (Eq. (3)), to:

$$\mathbb{E}\{\mathscr{L}_N(E_s)\} = \mathscr{L}_N(M)\mathscr{M}_0^{\gamma_k}(S^{-1}(H_s)). \tag{11}$$

Unfortunately, this simplistic vision cannot be extended to more complex measures such as the other LKCs that require structural information of the covariance function. The following section presents a fully developed version of Adler (2008) for $\sigma \neq 1$.

3.2. General formula

Let g_r be a Gaussian related correlated RF defined as in Eq. (3). Since Gaussian RFs are Gaussian related ($S = \mathrm{id}$), the following result is rather general. Let λ_2 be the second spectral moment of the underlying Gaussian RF, $H_s \in \mathbb{R}$ the hitting set and ω_i the volume of the unit i-ball. If E_s is the resulting excursion set, expectation of the LKCs can be computed as follows:

Expectation Formula

$$\mathbb{E}\{\mathscr{L}_j(E_s)\} = \sum_{i=0}^{N-j} \binom{i+j}{i} \frac{\omega_{i+j}}{\omega_i \omega_j} \left(\frac{\lambda_2}{2\pi}\right)^{i/2} \mathscr{L}_{i+j}(M)\, \mathscr{M}_i^{\gamma_k}(S^{-1}(H_s)). \tag{12}$$

It can be sensed that this relationship between, on the one hand the measure of the resulting excursion set and on the other hand, the hitting set and its probabilist characteristics, is strongly non linear. Hence, the end of this section focuses on developing it in a special case and analyzing the curves. Verifications of this theory on actual excursion sets are also presented and commented on.

Prior to that, it can be quickly checked that, in the one-dimensional case presented above, the Euler characteristic can be linked to the number of up-crossing levels defined Eq. (5):

$$\mathbb{E}\{\mathscr{L}_0\} = \mathscr{M}_0^{\gamma_k} + \mathbb{E}\{\mathcal{N}\}. \tag{13}$$

3.3. Physical interpretation and numerical aspect

In this section, Eq. (12) is developed for $g : C \subset \mathbb{R}^3 \to \mathbb{R}$ a correlated Gaussian RF of zero mean and σ^2 variance. Its covariance function is taken to be Gaussian with correlation

length l_c, making the second spectral moment $\lambda_2 = 2\sigma^2/l_c^2$. g is defined over a three-dimensional cube C of size $a \times a \times a$. The hitting set is the open subset of $\mathbb{R}$, $H_s = [\kappa, \infty)$ as above. LKCs of the resulting excursion set in these conditions can now be explicitly developed, in terms of κ:

Expected LKCs for Gaussian distribution

$$\mathbb{E}\{\mathscr{L}_0(E_s)\} = \left[\frac{1}{\sqrt{2}\pi^2}\frac{a^3}{l_c^3}\left(\frac{\kappa^2}{\sigma^2} - 1\right) + \frac{3}{\sqrt{2}\pi^{3/2}}\frac{a^2}{l_c^2}\frac{\kappa}{\sigma} + \frac{3}{\sqrt{2}\pi}\frac{a}{l_c}\right] e^{-\kappa^2/2\sigma^2} + \Psi\left(\kappa/\sigma\right) \quad (14a)$$

$$\mathbb{E}\{\mathscr{L}_1(E_s)\} = \left[\frac{\sqrt{2}}{\pi^{3/2}}\frac{a^3}{l_c^2}\frac{\kappa}{\sigma} + \frac{3}{2^{3/2}}\frac{a^2}{l_c}\right] e^{-\kappa^2/2\sigma^2} + 3a\Psi\left(\kappa/\sigma\right) \quad (14b)$$

$$\mathbb{E}\{\mathscr{L}_2(E_s)\} = \frac{\sqrt{2}}{\pi}\frac{a^3}{l_c} e^{-\kappa^2/2\sigma^2} + 3a^2\Psi\left(\kappa/\sigma\right) \quad (14c)$$

$$\mathbb{E}\{\mathscr{L}_3(E_s)\} = a^3\Psi\left(\kappa/\sigma\right) \quad (14d)$$

where Ψ is the complementary cumulative density function (tail distribution) of the Gaussian distribution.

Fig. (6) represents the volume fraction $\Phi = \mathscr{L}_3/a^3$ and the Euler characteristic $\chi = \mathscr{L}_0$ of excursion sets using a Gaussian distribution of zero means, variance $\sigma^2 = 25$ and Gaussian covariance of correlation length $l_c = 10$ for a large range of thresholds.

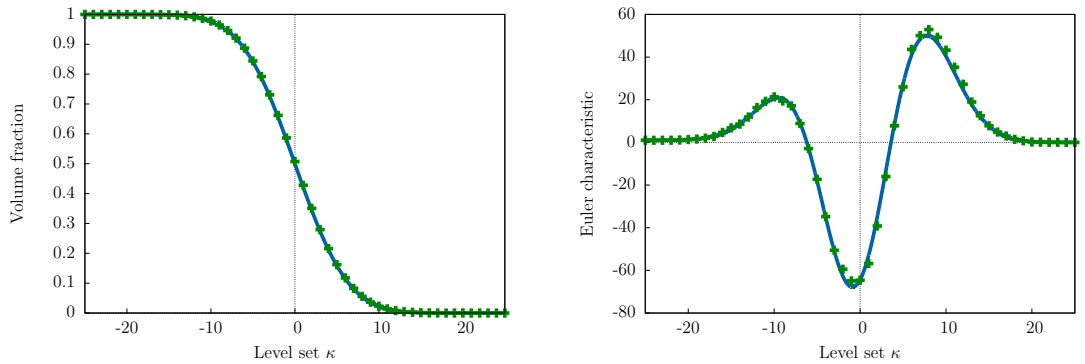

(a) Expected volume fraction Φ.

(b) Expected Euler characteristic χ.

Figure 6: Gaussian excursion set expected LKCs values for theoretical results (—) and actual realizations (+) over a range of thresholds ($a = 100, \sigma^2 = 25, l_c = 10$).

It has been seen in Eq. (14d) that the volume of an excursion is proportional to the tail probability of the underlying RF. Its constant decreasing shape clearly reflects the threshold effect on the excursion and its link with Gaussian measure γ_1. In other words, the volume fraction of the excursion is the Gaussian volume. Hence it is rather intuitive that its value is the tail distribution (see Fig. (7)). Even if more peculiar, the Euler characteristic curve shape also easily reflects the effect of the threshold on the excursion set's topology. For

values of κ lower than the lowest value of g, the Euler characteristic is that of the full cube C ($\mathscr{L}_0 = 1$). By increasing it, a closed porosity is represented (holes) leading to a positive value of the Euler characteristic ($\mathscr{L}_0 > 1$, see FIG. (7(a))). Then, the expansion of the holes starts to form handles which lead to a open porosity topology ($\mathscr{L}_0 < 0$, see FIG. (7(b))). By increasing κ even more, handles disappear forming a matrix/inclusion topology of connected components ($\mathscr{L}_0 > 0$, see FIG. (7(c))). Finally, the Euler characteristic decreases to $\mathscr{L}_0 = 0$ when no more connected components remain.

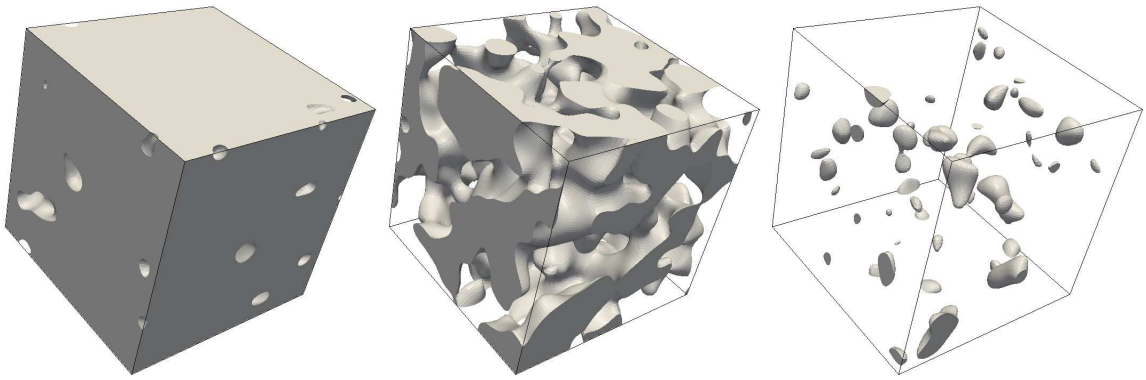

(a) $\kappa = -10$: Closed porosity. (b) $\kappa = 0$: Open porosity. (c) $\kappa = 10$: Matrix/inclusion.

Figure 7: Illustration of different topologies with three excursions from the same realization and different thresholds κ ($a = 100, \sigma = 5, l_c = 10$).

Though it is hard to tell for κ close to 0, $\mathscr{L}_0(\kappa \ll 0)$ and $\mathscr{L}_0(\kappa \gg 10)$ clearly correspond to the number of holes and the number of connected components, respectively, the other two topological features of EQ. (6) being absent.

From a numerical point of view, excursion sets are represented by a discretized binary field defined by 1 if in the excursion and 0 if elsewhere. Based on 100 realizations of excursions, average values of morphological characteristics are compared to theoretical means in FIG. (6). In addition to the validation of the theory, this statistical analysis also provides rather interesting information on the second moment. Herein, the very low variance of the LKCs insures that the characteristics of the excursions are not too spread around the expected values. In other words: it is insured that the morphological characteristics of *one* realization will be close to these targeted. Hence, the random aspect that the excursion set brings to any morphological model is only about the spatial repartition of the shapes, not about their characteristics, a key and necessary property.

A formula that links the probabilistic properties of the underlying RF and the hitting set with those characteristics has been given in this section. It predicts and controls, statistically speaking, the excursion set properties. In three dimensions, four measures are defined. Herein, focus is only made on the volume and the Euler characteristic, giving both geometrical and topological descriptors.

Attention is now drawn to applying it in order to model heterogeneities of concrete-like materials. Even though the model can yield morphologies adapted to the micro scale

(less than the $[\mu m]$) (open and closed porosity), only the meso-scale is considered here. Therefore, the morphology of interest is made of aggregates melt within a mortar matrix. Topologically speaking, a set of disconnected components needs to be modeled. Furthermore, this application is an opportunity to raise two main issues: *reaching high volume fractions with a disconnected topology* and *representing a grain size distribution.*

4. Application to meso-scale modeling of concrete

In this section, details on the morphological modeling of concrete-like material heterogeneities are given. A scale range has to be determined in order to define which kind of geometrical information is needed to be represented. Herein, focus is placed on the first scale below the macroscopic one referred to as the meso-scale. The length range taken into consideration goes from above the millimeter to hundreds of millimeters. At this scale, concrete-like material can be represented by two phases (each of them assumed to be homogeneous): the aggregates and the mortar. Hence a specific topology is considered in which disconnected inclusions are embedded within a mortar matrix. Several features of these morphologies, *e.g.* high volume fractions or grain size distribution, have to be tackled with attention, especially within the excursion set framework. Both aspects are now treated.

4.1. Reaching high volume fraction with disconnected topology

In order to understand the problematic of this section, it is recalled that several characteristics have to be taken into account when a morphology is considered (actually four in a three-dimensional space as seen above). Herein, only two of them are assumed to be relevant. The first characteristic is the volume fraction Φ and the second is the Euler characteristic χ. While the first grants a geometrical measure, the latter is used as an indicator of the topological rendering. The two others (one and two-dimensional measures) are let free. Due to the length range considered here, volume fractions higher than 30% are targeted. These values can easily be reached if no topological restrain is set. Actually, by choosing the right threshold, Eq. (14d) shows that any fraction can be computed from 0% to 100% (corresponding to $\kappa \to \infty$ and $\kappa \to -\infty$, respectively Fig. (6(a))). It becomes more complicated whether a second constrain appears, like in our case, the topology. As it has just been said, a disconnected morphology of inclusions within a matrix is wanted. It corresponds to high values of the threshold and therefore to low volume fractions. By considering the physical meaning of Euler characteristic (see Eq. (6)), this topology is quantified by positive values of χ due to components and not to holes. In Fig. (6(b)), it is located after the second zero, around the second local maximum. It can be checked in Fig. (6(a)) that indeed, these thresholds lead to low volume fractions. The quantity of interest is taken to be this second zero. This point is discussed with details in Roubin (2013), however, it can be admitted that it corresponds to the percolation of the excursion set. In other words, by taking κ decreasingly from infinity, it is when χ is first null that a path among the excursion is made between two faces. If κ_{p^+} is this threshold, it is assumed that all values greater than it are acceptable.

Before proceeding further, a handful length-scale ratio (α) of an excursion set is defined Eq. (15) by the ratio between the correlation length l_c and the domain size a[4]:

$$\alpha = \frac{l_c}{a}. \tag{15}$$

The graph in Fig. (8) draws expected values of χ in terms of κ for several ratios α (Euler characteristics are normalized $\mathbb{E}\{\chi\}/\max(\mathbb{E}\{\chi\})$ in order to represent them on the same graph). As mentioned above, attention is focused on κ_{p^+}, corresponding to $\chi = 0$ for $\kappa > 0$. Notice that, κ_{p^+} decreases along with the ratio α until a certain value where it is not defined anymore. An analysis of this feature is now proposed.

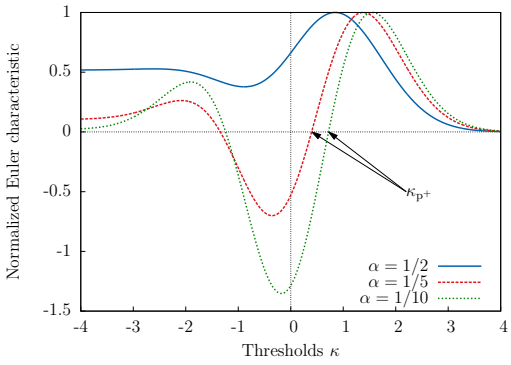

Figure 8: Expected values of the Euler characteristics in terms of thresholds for Gaussian excursion sets of unit variance and several ratios α.

First, notice can be made that the equation of the Euler characteristic Eq. (14a) is made of order three polynomial in α^{-1} (with no constant term) multiplied by an exponential to which the tail function is added. For very small α, only the first term of the polynomial can be retained, thus leading to a very simple expression of the Euler characteristic Eq. (16). Actually, this equation was discovered by Robert Adler in 1976 during his Ph.D. thesis. The other terms have been introduced by the late Keith J. Worsley Worsley (1996) and may be seen as *boundary corrections* or *boundary effects*.

$$\mathbb{E}\{\chi\} \approx \frac{1}{\sqrt{2}\pi^2}\frac{a^3}{l_c^3}\left(\frac{\kappa^2}{\sigma^2} - 1\right) e^{-\kappa^2/2\sigma^2}. \tag{16}$$

Hence, a null value of the Euler characteristic necessarily leads to $\kappa_{\mathrm{p}^+} = \sigma$. The corresponding volume fraction is then $\Phi = \Psi(1) \approx 16\%$. This case gives an accurate result for suitable topologies, although it is a lower bound. The graph in Fig. (9) draws the higher volume

[4]The following reasoning is based the impact of α on topological properties. However, notice that the resulting equation (Eq. (17)) is rather general and does not depend on the RF parameters (such as σ, l_c or a).

fractions, $\Phi(\kappa_{\mathrm{p}^+})$ (plain curve) in terms of the ratio α. The horizontal dashed line corresponds to the latter asymptotic value. It can be seen that by reducing the cube size, this volume fraction increases until a limit around $\alpha \approx 0.3$ depicted by the vertical dashed line (for a unit correlation length, it corresponds to a cube of size $a \approx 3.4$). Beyond this value, the expected Euler characteristic is always positive (see FIG. (8) for $\alpha = 1/2$). It can be understood by considering the other extreme case, for which an excursion set is considered in a very small cube. Simplification of EQ. (14a) tells that the Euler characteristic equals the tail probability and then, also equals the volume fraction. It can be interpreted as follows: if $\alpha \gg 1$ then the RF tends to be constant in space. Hence, an excursion is whether the cube itself or nothing. On an actual realization, $\chi(\kappa)$ would be a step function, getting from 1 to 0 discontinuously. It is the statistical expected value aspect that grants the smooth shape of $\mathbb{E}\{\chi(\kappa)\}$. Anyway, no further topological information can be withdrawn from these cases.

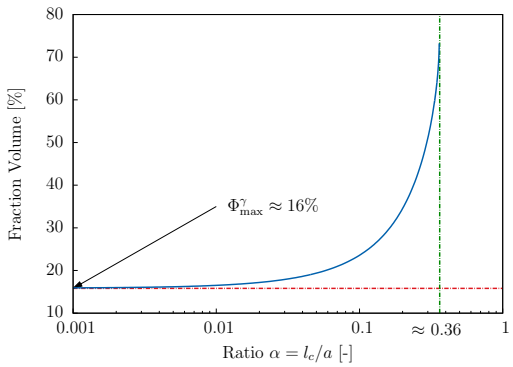

Figure 9: Higher volume fractions for disconnected topology.

Even if the volume fraction between the two extreme cases seems to be high enough on the graph, experiences have shown that, considering a higher ratio than $\alpha \approx 0.15$ leads to connected topologies even for thresholds slightly higher than κ_{p^+}. The side effects are too strong in these length-scales and the statistical meaning of expected percolation does not stand anymore. Discussion on that matter can be found in Roubin (2013) where these considerations leads to the determination of a Representative Volume Element for percolation. On the other hand, it is important to be able to represent volume fractions regardless any heterogeneity sizes. It is for these reasons that the maximal volume fraction is assumed to be the asymptotic value for infinite domains. Hence, for Gaussian distribution:

$$\Phi^{\gamma}_{\max} = 16\%. \tag{17}$$

In order to increase this value, a solution using χ^2_k distribution is now proposed.

First a χ^2 distribution with one degree of freedom ($k = 1$) is considered. If g is a Gaussian RF then $g_r = S(g) = g^2$ follows the χ^2_1 distribution. As seen during the presentation of excursion set theory, dealing with excursion sets of Gaussian related distribution falls down to a simple hitting set transformation S^{-1}. Herein, if the hitting set of interest is $H_s = [\kappa \ \infty)$ for χ^2_1, it becomes $S^{-1}(H_s) = (-\infty \ -\sqrt{\kappa}] \cup [\sqrt{\kappa} \ \infty)$ in the Gaussian point of view (notice

that now $\kappa > 0$ since g_r takes its value in $\mathbb{R}_+$). Basically, due to the symmetrical aspect of Gaussian distributions, the excursion set volume has doubled. This feature is represented with two-dimensional excursions in FIG. (10) where both Gaussian and corresponding χ^2_1 excursion are represented.

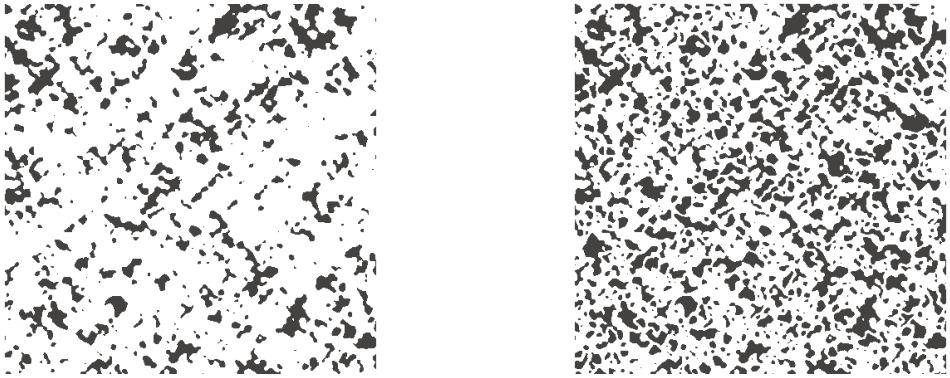

(a) Gaussian distribution: g. (b) χ^2_1 distribution: $g_r = g^2$.

Figure 10: Comparison between Gaussian and χ^2_1 excursion sets using the same underlying RF.

It is then only natural to stipulate that the maximum volume fraction has doubled too (it can easily be shown the same manner as for Gaussian distribution). Hence:

$$\Phi^{\chi^2_1}_{\max} = 32\%. \tag{18}$$

However, the behavior of excursion when $\kappa \to 0$ has to be tackled with caution. A topological discontinuity occurs at zero, corresponding to the transition between $S^{-1}(H_s) = \mathbb{R}^*$ and $S^{-1}(H_s) = \mathbb{R}$. In the first case, two completely disconnected parts of the excursion can be identified; the one from the lower part of $S^{-1}(H_s)$, $(-\infty \ -\sqrt{\kappa}]$ and the one from the upper part $[\sqrt{\kappa} \ \infty)$. These two phases connects together only when $\kappa = 0$, leading to a jump from a very low value of the Euler characteristic ($\chi < 0$) to a unit value ($\chi = 1$). It is proved that a regular behavior is obtained by increasing the number of degrees of freedom ($k \geq 5$), thus avoiding this discontinuity. However, herein, it is not the concern since κ is taken greater than κ_{p^+} (*i.e.* far from this discontinuity).

By analyzing the maximum volume fraction with several numbers of degrees of freedom of the χ^2_k distribution, it can be directly seen that the best case remains for $k = 1$. FIG. (11) shows for $\alpha = 0.001$: on the left, three curves representing the Euler characteristic with $k = 1, 2$ and 5 and their respective κ_{p^+} and on the right, the corresponding volume fractions $\Phi(\kappa_{\mathrm{p}^+})$ for $k = [1..25]$, showing its decreasing shape. For infinite number of degrees of freedom, it naturally tends to the Gaussian limit of 16% (central limit theorem). Finally, a χ^2_1 distribution is retained in order to model a disconnected topology. The precaution consisting in taking a threshold slightly higher than κ_{p^+} is taken in order to insure the desired topology. Determining all parameters of the morphological model can be decomposed in the following steps:

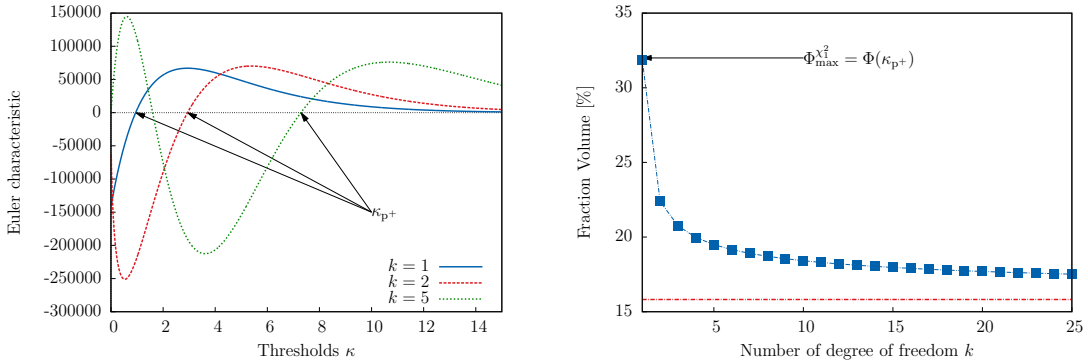

(a) Expected Euler characteristic of χ^2_k excursion set in terms of threshold.

(b) Volume fraction for $\kappa = \kappa_{p^+}$ in terms of number of degrees of freedom.

Figure 11: Maximum volume fraction in the χ^2_k case for a ratio $\alpha = 0.001$.

Step 1: Determination of the ratio κ/σ

Thanks to the previous analysis, the maximum volume computable for a suitable disconnected topology is known. For example let consider a targeted volume fraction of 20%. As depicted in Fig. (12(a)), Eq. (14d) gives the value of κ/σ. If a unit variance distribution is considered, then $\kappa_{20\%}$ is explicitly known. Notice that this step is independent of any length scale.

Now, in order to move on topological considerations, a length-scale has to be fixed. Depending on the problematic, Eq. (14a) can be used as described in step 2a or step 2b. It is recalled that for these disconnected topologies, the Euler characteristic represents the number of components.

Step 2a: Determination of the correlation length l_c

If no length-scale is imposed, a number of inclusions can be targeted. Since κ is determined during step 1, a simple inversion of Eq. (14a) for a given size a leads to a value of l_c. Note that choosing the volume fraction and the number of components leads to a single component size.

Step 2b: Determination of the number of inclusions

If a length-scale is imposed by the problem; for example inclusions of size 1 in a cube of size 1000, as shown in Fig. (12(b)), Eq. (14a) gives the expected number of inclusions $\chi \approx 44873$.

Unfortunately, this theoretical case is hardly computable (but not impossible) since the ratio $\alpha = 0.001$ implies a generation of heavily discretized correlated RFs. However, three-dimensional realizations of $200 \times 200 \times 200$ points can be computed in reasonable times (around a minute), thus representing accurately a length ratio of $\alpha = 0.01$. Examples in a cube of size $a = 100$ with $l_c = 1$ and 10 are shown in Fig. (13).

In this section it has been described how to double the maximum volume fraction of disconnected morphologies using a χ^2 distribution of one degree of freedom instead of a

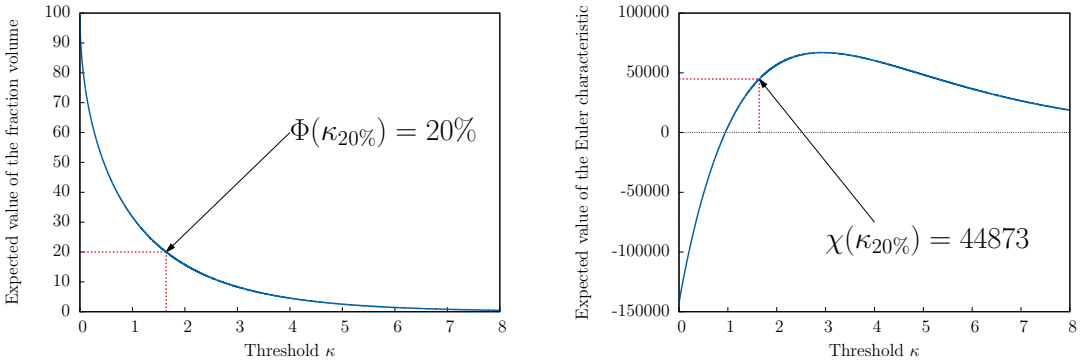

(a) Expected volume fraction. (b) Expected Euler characteristic.

Figure 12: Expected LKCs for χ^2_1 excursion set of unit variance and $\alpha = 0.001$. A volume fraction of 20% is targeted giving a corresponding Euler characteristic of 44873.

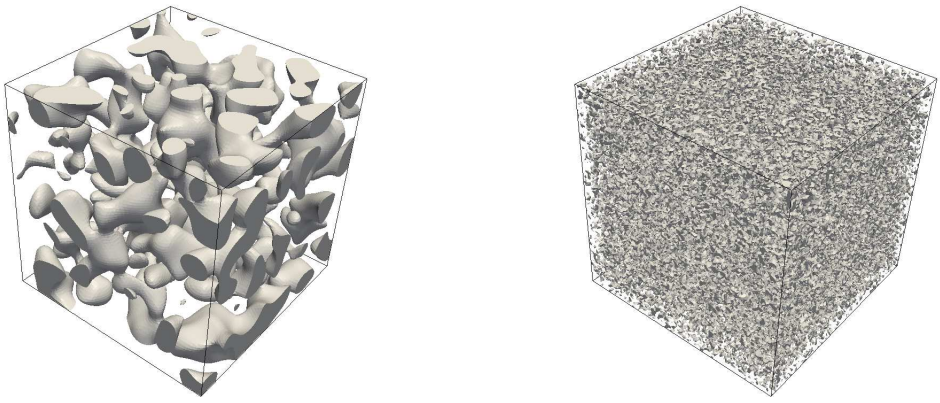

(a) $a = 100$ and $l_c = 10$. (b) $a = 100$ and $l_c = 1$.

Figure 13: Disconnected excursions with 20% volume fraction using a χ^2_1 distribution with two correlation lengths.

Gaussian one. A criterion independent from the length ratio α based on percolation of the excursion is used. With a certain margin to insure a suitable topology, it has been seen that 20% of volume fraction can easily be modeled. The following section gives directions on an additional method that combines several excursion sets with different correlation lengths in order to, on the one hand, increase the volume fraction even more and, on the other hand, represent a size distribution of the heterogeneities.

4.2. Modeling of the grain size distribution

Up to this point, only one characteristic length was considered for excursion sets. However, morphological modeling of aggregates has to be represented by heterogeneities that follow a given grain size distribution. Henceforth, the challenge is to yield a single excursion with different characteristic lengths and still to be able to control its geometrical and topological properties. The idea is to consider a set of K independent excursions $\{E^k_s\},\ k = [1..K]$

with their own characteristics. Among them, the most important characteristic is of course the correlation length l_c^k. And finally, the union of every excursions defines a new excursion which possesses multiple characteristic lengths. These excursions are referred to as:

$$E_s^{\cup} = \bigcup_{k=1}^{K} E_s^k. \tag{19}$$

Along with several hypothesis, the principle of measure of union of sets is used in order to estimate the different LKCs of the resulting excursion.

To begin with, a simple two-dimensional example is considered. Let E_s^1 and E_s^2 be two excursions of respective LKCs and correlation lengths $\{\mathscr{L}_n^1\}$, l_c^1 and $\{\mathscr{L}_n^2\}$, l_c^2. It is assumed that $l_c^1 > l_c^2$. Fig. (14(a)) represents the two excursions defined on the same domain, E_s^1 being in light grey and E_s^2 in dark grey while Fig. (14(b)) represents the union of both, *i.e.* $E_s^{\cup}$.

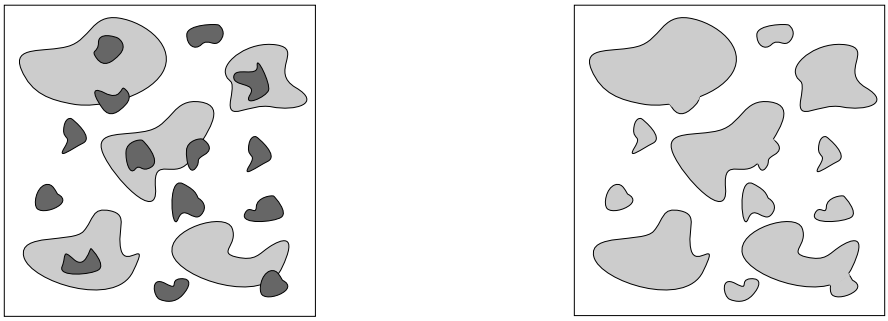

(a) Two excursion sets.

(b) Union of two excursion sets.

Figure 14: Illustration of the use of several excursions — two here.

In a more general case, attention is drawn to the calculation of each LKC $\mathscr{L}_n,\ n = [0..N]$ of $E_s^{\cup}$ in a N-dimensional space. Following the axiomatic that defines any measure, it can be yielded by:

$$\mathscr{L}_n(E_s^{\cup}) = \mathscr{L}_n(E_s^1 \cup E_s^2) = \mathscr{L}_n(E_s^1) + \mathscr{L}_n(E_s^2) - \mathscr{L}_n(E_s^1 \cap E_s^2). \tag{20}$$

Under hypothesis of sufficient ergodicity for the underlying RFs and statistically representative volumes (low length ratio α for both excursions) the assumption that the k^{th} measure of the intersection is approximated by the actual measure of the lower correlation length excursion pondered by the specific value of the last LKC of the higher one (the specific surface area in two dimensions or the fraction volume in three dimensions) can be made. It leads to a completely predictable approximation of each measure of the union:

$$\mathscr{L}_n(E_s^{\cup}) = \mathscr{L}_n(E_s^1 \cup E_s^2) \approx \mathscr{L}_n(E_s^1) + \mathscr{L}_n(E_s^2)\left(1 - \Phi_N(E_s^1)\right), \tag{21}$$

$\Phi_N(E_s^1) = \mathscr{L}_N(E_s^1)/\mathscr{L}_N(M)$ being the specific value.

Under the same assumptions, the generalization of this principle to the union of more than two excursions is rather straightforward. If K excursions are considered with different *sorted* correlation lengths ($l_c^1 > \cdots > l_c^k > \cdots > l_c^K$), using a recursive process on Eq. (20), the LKCs can be computed:

$$\mathscr{L}_n(E_s^{\cup}) \approx \mathscr{L}_n(E_s^1) + \sum_{k=2}^{K} \mathscr{L}_n(E_s^k) \left(1 - \bigcup_{l=1}^{k-1} \Phi_N(E_s^l)\right), \tag{22}$$

in which, thanks to the Poincaré formula and the approximation made in Eq. (21), the union of Φ_N can be computed as follows:

$$\bigcup_{k=1}^{K} \Phi_N(E_s^k) \approx \sum_{k=1}^{K} \left((-1)^{k-1} \sum_{1 \le i_1 < i_2 < \cdots < i_k \le K} \Phi_N(E_s^{i_1}) \Phi_N(E_s^{i_2}) \ldots \Phi_N(E_s^{i_k})\right). \tag{23}$$

Finally, since measures of each excursion set E_s^k are predictable, expected values of the LKCs, $\mathbb{E}\{\mathscr{L}_i(E_s^{\cup})\}$ can now be computed. It is recalled that Eq. (22) is an approximation. Hence, comparison with experimental results is recommended. Three excursions using a χ_1^2 distribution and characteristic lengths $l_c = 10, 5$ and 2 are defined in a three-dimensional cube of size $a = 100$. Both Euler characteristic $\chi = \mathscr{L}_0$ and volume fraction $\Phi = \mathscr{L}_3/a^3$ of the resulting excursion are compared to the analytical approximation Eq. (22). Results are drawn in Fig. (15). Notice that, even if not mandatory, for the sake of handful representation, the excursion set is the resulting union of excursion sets obtained with the same threshold.

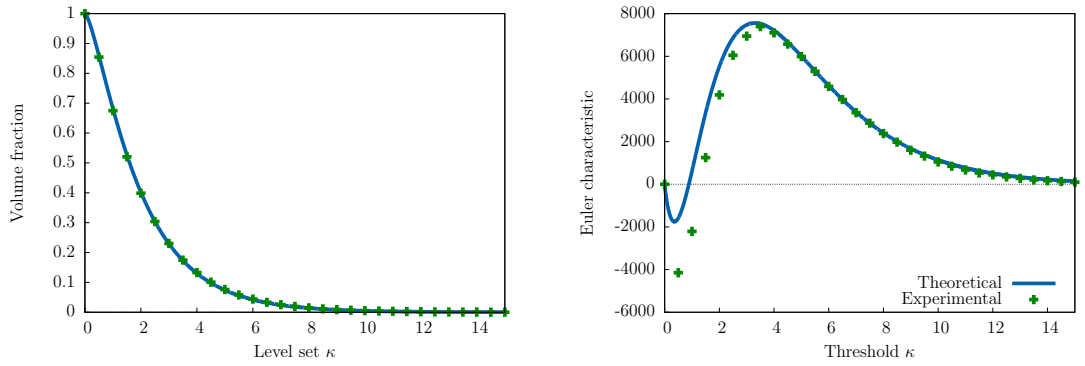

Figure 15: Union of χ_1^2 excursion set expected LKCs values for theoretical results (—) and actual realizations (+).

It can be seen directly that the approximation for the volume fraction is rather good. However, the theoretical Euler characteristic is overestimated for low thresholds. It can be explained by a too coarse spatial discretization in regards with the discontinuous aspect of χ_1^2 excursion sets for $\kappa = 0$ which is numerically hard to catch. Anyway, regarding disconnected topology, the maximum number of particles is well estimated, as for the decreasing part of the curve. Another important feature that unions enable is that the computable volume

fractions are higher than while using a single excursion. Notice that on the presented example the volume fraction is around 50% for κ_{p^+}. As a precaution, the threshold is taken so that $\kappa \gg \kappa_{\mathrm{p}^+}$, leading to excursion sets of, for example, 40% volume fraction and disconnected topology[5].

The morphological modeling of a set of *only one class* particles can be made by using an excursion set with a *single* correlation length chosen in the range $D_{\min} < l_c < D_{\max}$ ($D_{\min|\max}$ being extreme diameters of the class). It is assumed that a distribution of disconnected particles which sizes are spread around the correlation length produces an acceptable representation of one class. Therefore, for now on, $l_c = \frac{1}{2}(D_{\max} + D_{\min})$. It can be extended to several classes using unions of excursion sets in which each excursions of the union represents a single class. To follow a given distribution of sizes (granulometry), the volume fraction of each excursion has now to be determined.

In order to fit in the numerically computable range of a cube of size $a = 100\,mm$, only medium ($D_{\max} = 16\,mm$), fine ($D_{\max} = 8\,mm$) and very fine gravels ($D_{\max} = 4\,mm$) are considered and particles lower than $2\,mm$ are considered part of the mortar matrix. For a total volume fraction of $\Phi = 40\%$ it is assumed that the granulometry gives the following Volume fractions $\Phi^{\{1,2,3\}} = \{0.25\Phi, 0.5\Phi, 0.25\Phi\}$, respectively. The correlation length of each class is taken to be the average of each class extrema diameters giving $l_c^{\{1,2,3\}} = \{12\,mm, 6\,mm, 3\,mm\}$, respectively. With regards to the union set theory, volume fractions of each excursion set will have to be targeted higher than the wanted value. In this case, they are computed as follows:

$$\Phi^1_{\text{target}} = \Phi^1 = 0.25\Phi \tag{24a}$$

$$\Phi^2_{\text{target}} = \frac{\Phi^2}{1-\Phi^1} = \frac{0.5\Phi}{1-0.25\Phi} \tag{24b}$$

$$\Phi^3_{\text{target}} = \frac{\Phi^3}{(1-\Phi^1-\Phi^2)} = \frac{0.25\Phi}{(1-0.75\Phi)} \tag{24c}$$

For a qualitative analysis, three realizations of this morphology are shown in Fig. (16) and a two-dimensional slice in Fig. (17(a)). From these pictures, it can be seen that the random aspect of excursion sets and the union procedure gives more "realistic" morphologies than with simple geometrical objects (like a hard sphere representation). More realistic in the sense that the local curvature can be significantly high ($\ll 0$) and low ($\gg 0$) which lead to locally convex and saddle surface. From a mechanical point of view (especially in regards to fracture), it is known that these geometrical properties lead to significant stress localization and therefore represents. Therefore it is a strong asset of this model (see Roubin et al. (2015)).

[5]At this stage, it is wise to base any morphological modeling using union of RF on the volume fraction and consider the percolation aspect more as an indicator than a reliable value. Finally, higher values of the threshold than those estimated are recommended in order to model disconnected topologies.

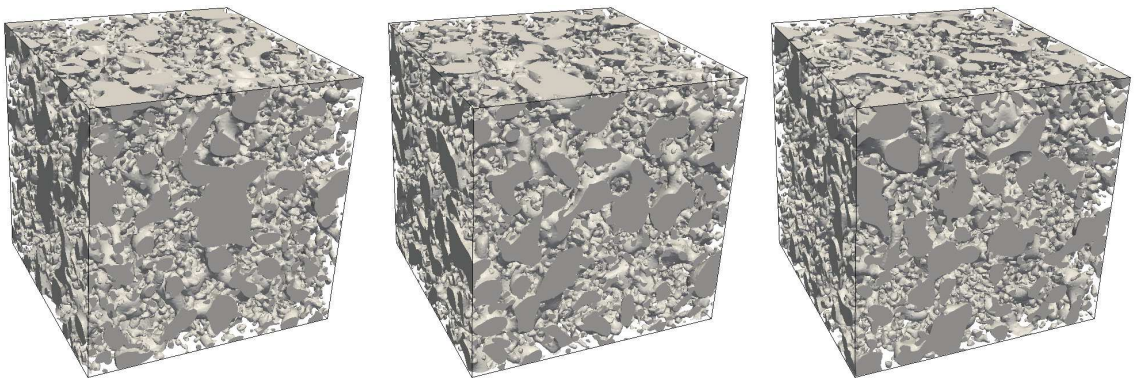

Figure 16: Three realizations of 40% volume fraction excursion sets of correlation lengths $\{12, 6, 3\}$.

However, comparing Fig. (17(a)) and (b) it can be observe that some gaps still exist between the model and the real material (here observed through X-ray tomography). The first one is the filtering of the smallest aggregates (small sand particles). Clearly this difference between the two images is linked to the possibility to compute realizations of Random Fields with very small covariance lengths (compared to the whole domain size), and thus on very fine grids. The second gap is mainly due to the infinitely derivative aspect of Gaussian covariance functions, the general aspect of aggregate being unrealistically smooth. On that matter, possible investigation directions are proposed in the conclusion.

(a) Excursion set extracted from Fig. (16).

(b) Segmented X-ray microtomography from Qier (2014).

Figure 17: Two-dimensional slices of diameter $8\,mm$: Comparison between excursion set and X-ray microtomography.

In order to perform a more qualitative analysis of the excursions obtained, a reconstruction of the grain size distribution using a morpho-mathematical method (which basically consists in performing a sequence of morphological opening with increasing size of the structuring element (Klein and Serra (1972)) is shown Fig. (18). Once again it can be seen that the computational limit leads to an important bias due to the presence of small particles ($D < 2\,mm$). However, considering larger sizes, the proportions of each class of aggregates

are rather well respected.

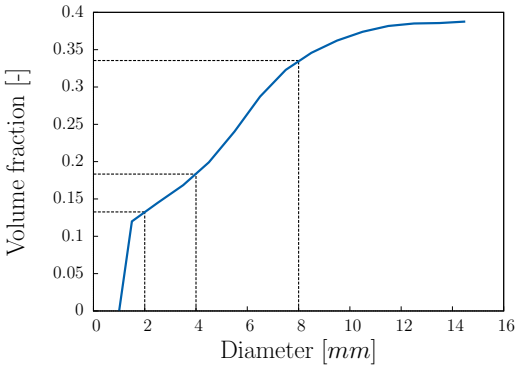

Figure 18: Reconstruction of the grain size distribution of one realization presented Fig. (16).

5. Concluding remarks

A morphological model based on excursion set of correlated RFs that produces complex randomly shaped morphologies has been presented. Original formulae Adler (2008) that statistically control the geometrical and topological characteristics of these excursion sets — volume, surface area, Euler characteristic — in terms of the RF parameters — correlation length, variance — has been adapted in order to model cementitious material heterogeneities at meso-scale. It has led to several problematics such as reaching high fraction volumes and representing a grain size distributions.

The main advantage of this class of morphological model is to allow for very different shapes (thinking of inclusions melt into a matrix) at once. However, as it has been pointed out, one of the main issue related to the excursion sets methodology is to reach high volume fractions while keeping a disconnected topology. Even if the use of another distribution — χ^2 rather than Gaussian — helped double it, the maximal compacity obtained with a single characteristic length in a representative volume is about 30 %. However, it was shown that by only considering a certain part of a grain size distribution (mainly gravels) and using union of excursion sets, relevant modeling can be obtained. Nonetheless, as presented during the introduction of this chapter, this value is lower than what an efficient poly-disperse sphere packing algorithm can produce. Dealing with that matter, a further work on hitting sets can be thought. An idea would be to extend the principle of χ^2 distribution to higher order, yielding vectors valued RF. Hitting sets shall be based on spherical harmonics functions, hence, as transforming the one-dimensional open hitting set $[\kappa, \infty)$ into the complementary ball of the same dimension double the volume fraction, working with hitting sets in higher dimensions should increase it as well.

An improvement of the method can also be made by considering all the excursion set characteristics. In this chapter, attention has mainly be focused on the volume fraction and

the Euler characteristic, which seem the more relevant characteristics to control first. In order to model the heterogeneities more accurately, it is recalled that in the three-dimensional space, information on two and one-dimensional measures such as surface area and calliper diameter, respectively, are also available. An analysis of the link between the latter and the correlation length could be an interesting research area.

Dealing with cementitious materials, it has been show that meso-scale (aggregates within a mortar matrix) can efficiently be represented, up to the computational limit associated to the RF simulation. Some works are now in progress dealing with a finer point of view for cement paste as a nano-porous material. Here the thresholds associated to the excursions are negative and, thus providing a "sponge-like" topology. Moreover, the excursion sets methodology presents major advantages when dealing with evolving microstructure in time. This is the case when considering cement hydration for which we think that this class of morphological model is really useful.

6. Acknowledgment

The research leading to these results has received funding from the European Research Council under the European Union's Seventh Framework Programme (FP/2007-2013) / ERC Grant Agreement n. 320815, Advanced Grant Project COMP-DES-MAT. The authors would also like to thanks the École Normale Supérieur de Cachan (FR) for the funding of one researcher at the early stage of this study.

References

Adler, R., 1981. The geometry of random fields. Classics in applied mathematics. Society for Industrial and Applied Mathematics (SIAM, 3600 Market Street, Floor 6, Philadelphia, PA 19104).

Adler, R., 2008. Some new random field tools for spatial analysis. Stochastic Environmental Research and Risk Assessment 22 (6), 809–822.
URL http://dx.doi.org/10.1007/s00477-008-0242-6

Adler, R. J., Taylor, J. E., Worsley, K. J., 2010. Applications of Random Fields and Geometry: Foundations and Case Studies.

Bezrukov, A., Bargiel, M., Stoyan, D., May 2002. Statistical analysis of simulated random packings of spheres. Particle & Particle Systems Characterization 19 (2), 111.

Federer, H., 1959. Curvature measures. Transactions of the American Mathematical Society 93 (3), pp. 418–491.
URL http://www.jstor.org/stable/1993504

Garboczi, E. J., Bentz, D. P., 1998. Multiscale analytical/numerical theory of the diffusivity of concrete. Advanced Cement Based Materials 8 (2), 77 – 88.
URL http://www.sciencedirect.com/science/article/pii/S1065735598000108

Kerscher, M., Mecke, K., Schuecker, P., Bohringer, H., Guzzo, L., Collins, C. A., Schindler, S., De Grandi, S., Cruddace, R., Oct. 2001. Non-gaussian morphology on large scales: Minkowski functionals of the REFLEX cluster catalogue. Astronomy and Astrophysics 377 (1), 1–16.
URL http://dx.doi.org/10.1051/0004-6361:20011063

Klein, J. C., Serra, J., Apr. 1972. The texture analyser. Journal of Microscopy 95 (2), 349–356.
URL http://doi.wiley.com/10.1111/j.1365-2818.1972.tb03734.x

Matheron, G., 1975. Random sets and integral geometry. Wiley series in probability and mathematical statistics: Probability and mathematical statistics. Wiley.

Mecke, K., Wagner, H., 1991. Euler characteristic and related measures for random geometric sets. Journal of Statistical Physics 64 (3-4), 843–850.
URL http://dx.doi.org/10.1007/BF01048319

Mecke, K. R., Buchert, T., Wagner, H., 1994. Robust morphological measures for large-scale structure in the universe. Astronomy & Astrophysics 288, 697–704.
URL http://arxiv.org/abs/astro-ph/9312028

Qier, W., 2014. Isothermes de d'adsorption de matériaux cimentaires : tude d'un protocole accéléré et estimation du ver. Ph.D. thesis, Universite Lille 1, Lille.

Rasmussen, C., Williams, C., 2006. Gaussian Processes for Machine Learning. Adaptative computation and machine learning series. University Press Group Limited.
URL http://books.google.fr/books?id=vWtwQgAACAAJ

Roberts, A., Garboczi, E., Oct. 1999. Elastic properties of a tungsten–silver composite by reconstruction and computation. Journal of the Mechanics and Physics of Solids 47 (10), 2029–2055.
URL http://linkinghub.elsevier.com/retrieve/pii/S0022509699000162

Roubin, E., Oct. 2013. Meso-scale FE and morphological modeling of heterogeneous media: applications to cementitious materials. Theses, École normale supérieure de Cachan - ENS Cachan, LMT-Cachan.
URL https://tel.archives-ouvertes.fr/tel-00957377

Roubin, E., Vallade, A., Benkemoun, N., Colliat, J.-B., Jan. 2015. Multi-scale failure of heterogeneous materials: A double kinematics enhancement for embedded finite element method. International Journal of Solids and Structures 52, 180–196.
URL http://linkinghub.elsevier.com/retrieve/pii/S0020768314003710

Rougelot, T., Burlion, N., Bernard, D., Skoczylas, F., 2010. About microcracking due to leaching in cementitious composites: X-ray microtomography description and numerical approach. Cement and Concrete Research 40 (2), 271 – 283.

Serra, J. P., 1982. Image analysis and mathematical morphology. Academic Press, London ; New York.

Stein, M., 1999. Interpolation of Spatial Data: Some Theory for Kriging. Springer Series in Statistics. Springer New York.

Taylor, J. E., 2001. Euler characteristics for gaussian fields on manifolds. Ph.D. thesis, McGill.

Taylor, J. E., Feb. 2006. A gaussian kinematic formula. The Annals of Probability 34 (1), 122–158.

Taylor, J. E., Adler, R. J., 2003. Euler characteristics for gaussian fields on manifolds. Annals of Probability 31 (2), 533–563.
URL http://projecteuclid.org/euclid.aop/1048516527

Winitzki, S., Kosowsky, A., Oct. 1997. Minkowski functional description of microwave background gaussianity. New Astronomy 3 (2), 75–99.
URL http://dx.doi.org/10.1016/s1384-1076(97)00046-8

Worsley, K. J., 1996. The geometry of random images. CHANCE 9 (1), 27–40.
URL http://www.tandfonline.com/doi/abs/10.1080/09332480.1996.10542483

Wriggers, P., Moftah, S., 2006. Mesoscale models for concrete: Homogenisation and damage behaviour. Finite elements in analysis and design 42 (7), 623–636.

Zhu, Q., Kondo, D., Shao, J., Mar. 2008. Micromechanical analysis of coupling between anisotropic damage and friction in quasi brittle materials: Role of the homogenization scheme. International Journal of Solids and Structures 45 (5), 1385–1405.
URL http://linkinghub.elsevier.com/retrieve/pii/S002076830700399X

Zubelewicz, A., Rougier, E., Ostoja-Starzewski, M., Knight, E., Bradley, C., Viswanathan, H., Dec. 2014. A mechanisms-based model for dynamic behavior and fracture of geomaterials. International Journal of Rock Mechanics and Mining Sciences 72, 277–282.
URL http://linkinghub.elsevier.com/retrieve/pii/S1365160914002561